Global Ecosystems and Environment Observation Analysis Report Cooperation (GEOARC) 2017

The Belt and Road Initiative Ecological and Environmental Conditions

National Remote Sensing Center of China
Ministry of Science and Technology of the People's Republic of China



To support global change studies and international cooperation in Earth Observation System of Systems (GEOSS), from 2012, the National Remote Sensing Center of China (NRSCC), Ministry of Science and Technology of the People's Republic of China has integrated a series of products from National Research and Development Program to continuously produce and release reports from Global Ecosystems and Environment Observation Analysis Report Cooperation (GEOARC).

As part of GEOARC–2017, taking 10 land regions and 12 ocean regions along the 'Belt and Road' as the monitoring area, a comprehensive analysis was conducted in various aspects, including the conditions of terrestrial ecosystems, ecological environment and development conditions of critical urban areas, road connectivity conditions, status of terrestrial solar energy resources, terrestrial water budge, and typical Marine disasters in key ocean areas. The data and report are published at the website of National Integrated Earth Observation Data Sharing Platform (http://www.chinageoss.org/geoarc/index.html).

Foreword

In this report, the monitoring land region covers Asia, Africa, Europe and Oceania, which can be divided into 10 sub–regions, i.e. West Asia, South Asia, East Asia, Southeast Asia, Central Asia, Russia, Oceania, Europe, Northern Africa and Southern Africa for facilitating regional comparative analysis. The monitoring sea area includes 3 oceans, Northwest Pacific ocean, Southwest Pacific ocean and Indian oceans, and 9 coastal areas, vis–a–vis Sea of Japan, East China Sea, South China Sea, Java–Banda Sea, Bay of Bengal, Arabian Sea, Mediterranean Sea, Black Sea and North Sea.

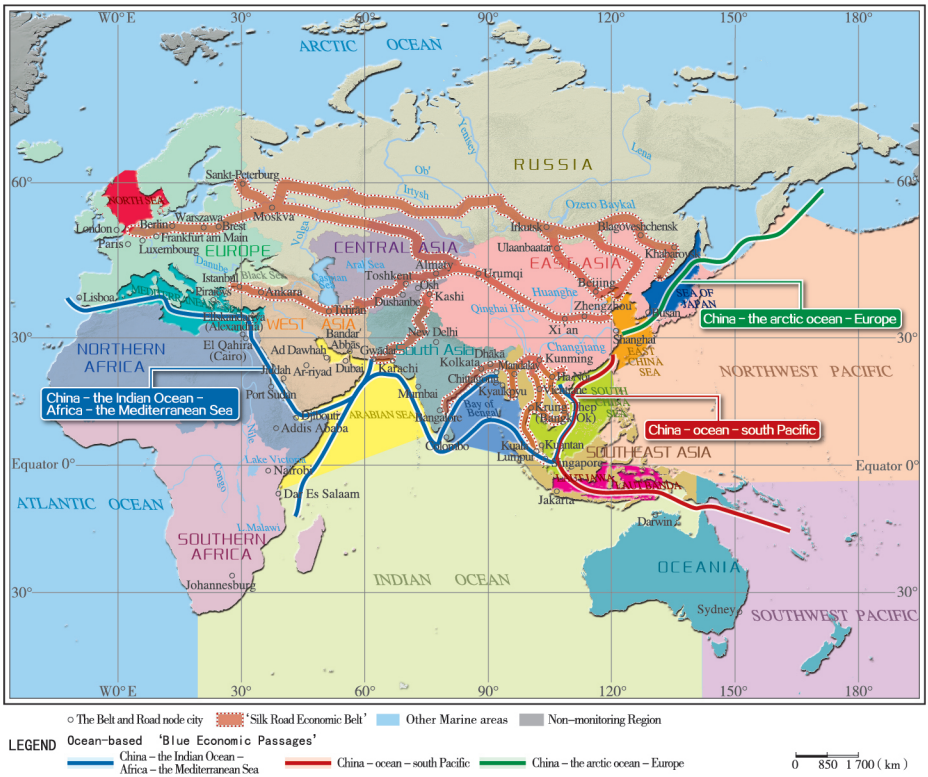

The remote sensing monitoring regions of the ecological environment over the 'Belt and Road' , key ocean areas (3 oceans and 9 coastal areas) and distributions of the three ocean–based 'Blue Economic Passages'

Using multi-source remote sensing data to derive 12 types of thematic data products to monitor ecological environment, i.e. the global land cover, leaf area index, fractional vegetation coverage, forest aboveground biomass, global solar radiation, evapotranspiration, water deficit, urban heat island index, road network density, disastrous wave, sea level anomalies and typhoon disaster. The report mainly analyzes the baseline ecological environment in 2015 and the dynamic change in recent years.

1. The conditions of terrestrial ecosystems

1.1 Macrostructure of ecosystems

The ecosystems in the monitoring area mainly include forest, desert, grassland, farmland, water and urban ecosystems, with forest being the largest ecosystem (occupying 32.15 million km^2), followed by desert, grassland and farmland (respectively 22.31 million km^2, 21.70 million km^2, 13.89 million km^2). Water ecosystems occupy some 2.00 million km^2. The least spatially extensive is the urban ecosystems with 0.52 million km^2. Significant differences are found in the ecosystem structure among the various sub-regions. Southeast Asia, Southern Africa, Russia, Oceania and Europe are dominated by forest ecological types, while the prevailing ecosystems of Central Asia and Northern Africa are grassland and desert ecosystems. South Asia is dominated by farmland, and the distribution of farmland, forest, grassland and desert ecosystems in East Asia is relatively in balance (Table 1-1, Fig. 1-1).

Table 1-1 The ecosystem area for each sub-region of the 'Belt and Road' monitoring area (unit: 10^4 km^2)

	Farmland	Forest	Grassland	Water	Urban	Desert
Russia	203.28	786.38	584.54	62.74	2.04	41.12
Europe	140.11	254.88	148.76	19.52	16.79	6.56
Southeast Asia	81.4	322.46	25.13	9.41	4.33	5.02
East Asia	177.47	318.54	272.11	35.18	14.08	349.52
South Asia	190.14	118.49	62.04	15.96	4.07	108.94
West Asia	83.63	36.4	67.86	4.56	2.9	420.21
Central Asia	20.87	12.37	226.18	14.38	0.68	125.73
Northern Africa	182.51	135.02	224.26	4.26	1.34	886.07
Southern Africa	292.28	862.19	343.56	27.46	4.92	43.11
Oceania	17.83	368.02	215.63	6.09	1.32	244.51

Fig. 1–1 Regional ecosystems over the 'Belt and Road' region in 2015

1.2 Productivity potential and stress of vegetated ecosystems

Photosynthetically active Radiation–Temperature–Vapor pressure deficit (PRTV) stress factor has profound implications on the spatial distribution and growth conditions of vegetation (Fig.1–2 and Fig.1–3). The Light–Temperature–Water(LTW) productivity potential varies considerably across the monitoring area. The condition is most favorable in the Congo River Basin in Africa and Southeast Asia and LTW productivity potential reaches the highest (about 120 t/ha). The LTW

productivity potential drops sharply to 50 t/ha in the tropical desert and subtropical desert ecological areas of the Northern Africa, Western Asia and western Australia mainly due to water limitation. Temperature and illumination stress factors limit vegetation growth in boreal forests, conifer, temperate grassland and forest of northern tundra biome with cold climate north of 40° N of Eurasia, where the LTW productivity potential is lower than 30 t/ha.

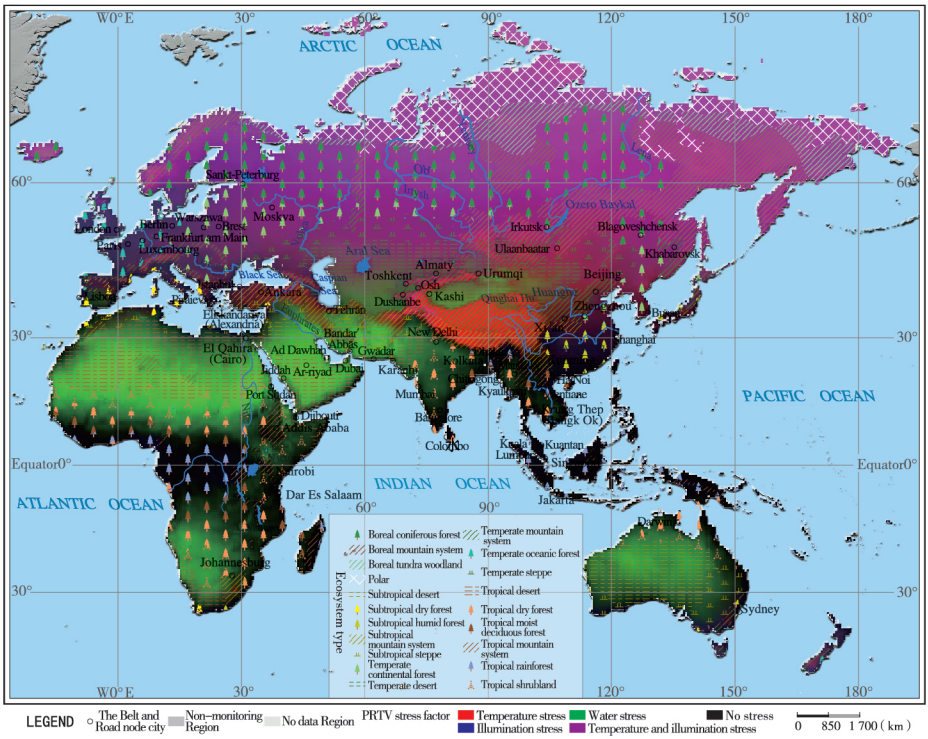

Fig. 1–2 PRTV stress factor of vegetation growth in the 'Belt and Road' region

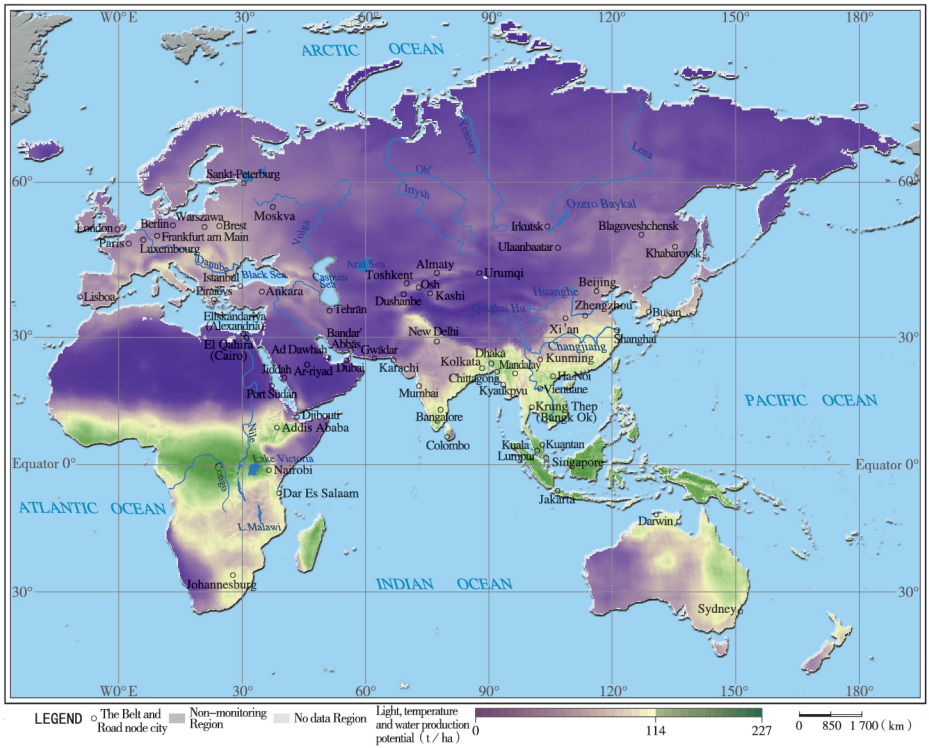

Fig. 1–3 Distribution of LTW productivity potential over the 'Belt and Road' region in 2015

1.3 Status of forest ecosystem

In the 'Belt and Road' regions forest areas are mainly distributed in Russia, Southern Africa, Europe, East Asia, and Southeast Asia. The forest aboveground biomass in the whole region was estimated to be 281.3 billion tons in 2015 (Fig. 1–4), an increase of about 1% over 2010. The proportion of the forest aboveground biomass in each region was 32.82% in Russia, 26.71% in Southern Africa, 10.59% in Europe, 8.80% in East Asia and 7.74% in Southeast Asia, and the incremental changes respectively 2.32%, –1.38%, 0.57%, 7.58% and –2.33% for each region (Fig. 1–5). The largest increase was found in East Asia, mainly attributed to afforestation activities. The decrease in biomass observed in South Africa and Southeast Asia is

mainly attributing to deforestation and forest fires. The tropical rainforests of northern Eurasia and boreal forest, central South Africa and Southeast Asia are an important part of the global forest Carbon Stock. Among them, in the cold temperate zone and cold zone in the northern Eurasian continent the carbon stock is the largest, but due to shorter growing seasons, the average annual leaf area index (ALAI) is low, so is the forest carbon sequestration capacity. The tropical rainforests near the equator in central and southern Africa and Southeast Asia, with the highest average ALAI and forest biomass, are the most productive forest ecosystems in the 'Belt and Road' region.

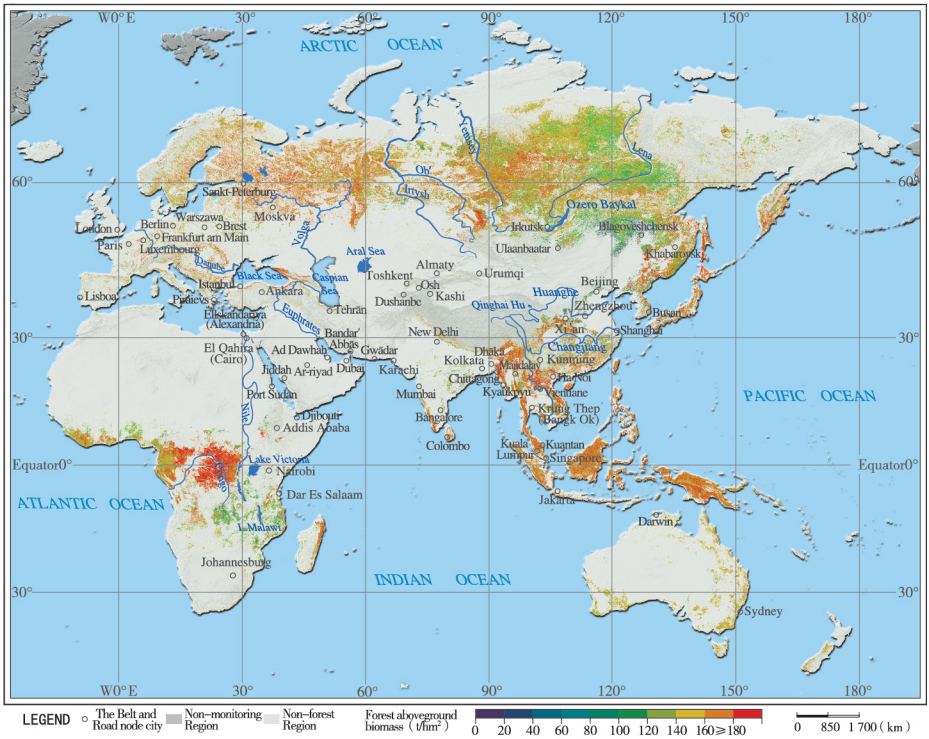

Fig. 1–4 Distribution of the forest aboveground biomass over the 'Belt and Road' region in 2015

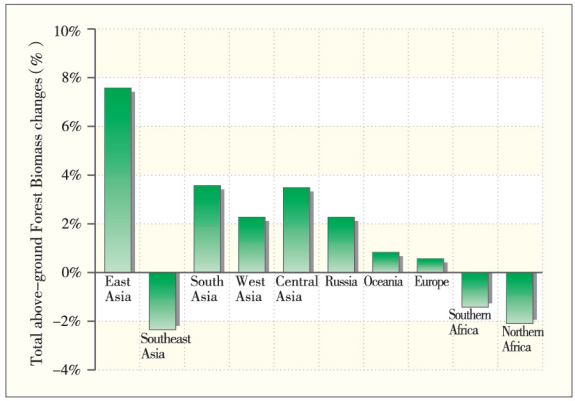

Fig. 1–5 Changes of the forest aboveground biomass of the 'Belt and Road' region in 2015 compared to 2010

1.4 Status of grassland ecosystems

Grassland ecological types within the 'Belt and Road' region are predominately distributed in the Mongolian plateau, southern Europe, southern Africa and northern Australia (Fig. 1–6). Under adequate LTW conditions in southern Russia, European temperate grassland and central and southern African savanna, the annual Maximum Fractional Vegetation Coverage(MFVC) and the ALAI are higher, while the annual ALAI is lower over northern tundra of northern Russia due to temperature and illumination stress factors and over alpine grassland Tibetan plateau due to relatively shorter growth period, although the MFVC is higher in summer. Constrained by the water stress factor, the annual MFVC and annual ALAI were lower in the southern margin of sub–Sahara Africa. The *El Niño* in 2015 resulted in decline in rainfall and drier climates in central and southern Africa and tropical region north of Australia, and decline of the annual ALAI by 3.79%. Meanwhile, the annual MFVC of the grassland has increased by 7.51% in the temperate grasslands of Central Asia and the tundra in northwestern Russia due to increased precipitation.

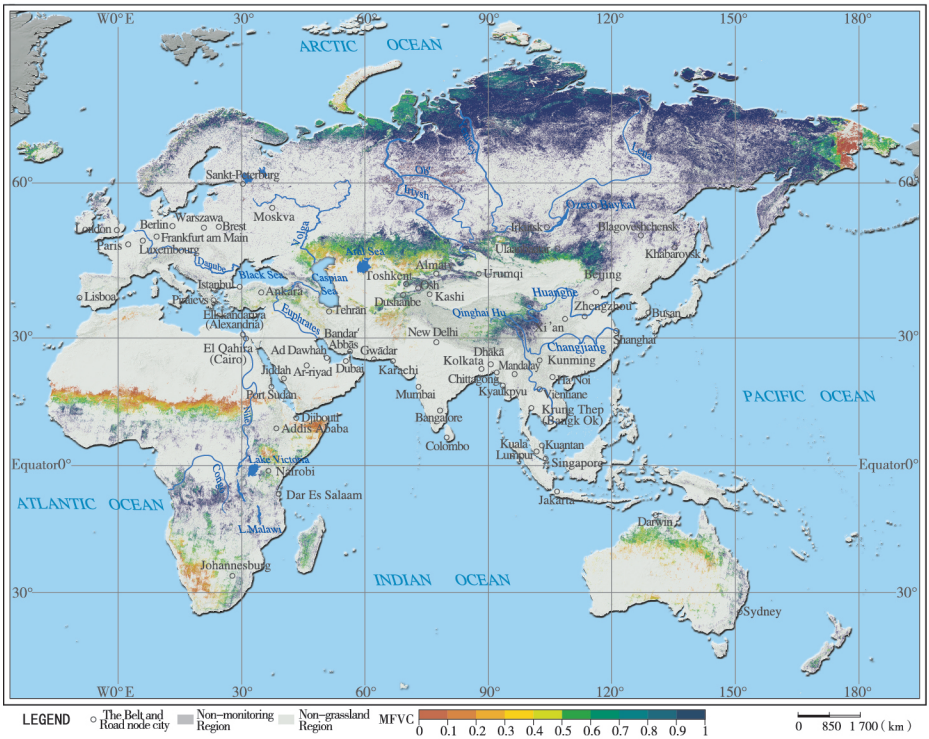

Fig.1–6 Distribution of the grassland annual MFVC over the 'Belt and Road' region in 2015

1.5 Status of farmland ecosystems

Farmland ecosystems are mainly distributed in western Russia, Southeast Asia, South Asia, east part of East Asia, Europe and South Australia (Fig. 1–7). Southeast Asia is endowed with multiple cropping seasons, and the annual ALAI is higher than 2, the highest within the 'Belt and Road' region. South Asia and Oceania are dominated by single cropping season, with an annual ALAI of less than 1. Affected by *El Niño* in 2015, in European corn and wheat producing region, south Asian rice producing region and south Australia farmland region, the annual ALAI decreased by 0.1–0.5 due to droughts, resulted in reduction in yield of maize, rice, wheat and soybean by 1.8%–6.9%.

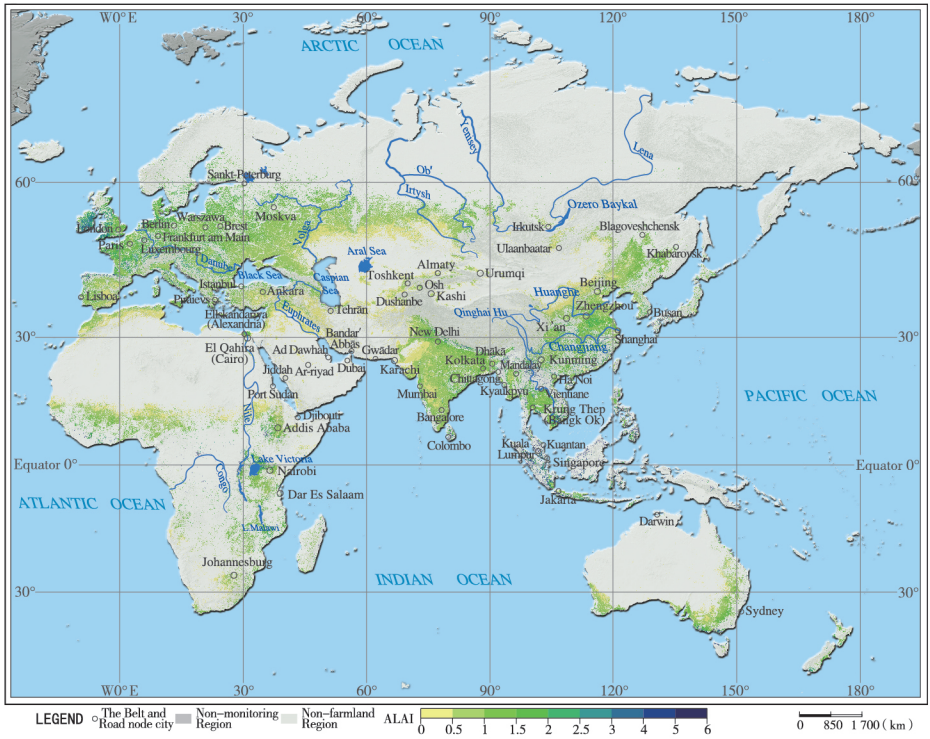

Fig.1–7 Distribution of annual ALAI of the farmland over the 'Belt and Road' region in 2015

1.6 Status of the vegetated ecosystems

The difference of vegetation growth condition in sub-regions is remarkable (Table 1-2). In 2015, the maximum forest aboveground biomass in Russia is estimated at 92.3 billion tons, and the annual ALAI and MFVC of forest in the Southeast Asia are the highest, being at 3.64 and 0.99 respectively. The annual ALAI of grassland and farmland in the southeast Asia region are the highest, 2.67

and 2.05 respectively, with the highest MFVC of 0.97 and 0.93.

From 2010 to 2015, the forest aboveground biomass increased by 2.1 billion tons and 1.7 billion tons respectively over Russia and East Asia, but decreased in Southern Africa, Southeast Asia and Northern Africa (1.1 billion tons, 500 million tons and 200 million tons, respectively). The annual ALAI of grassland in Russia and Oceania decreased by 0.52% and 3.79% respectively, and that of farmland in Oceania region decreased by 1.97% (Table 1–3).

Table 1–2 The conditions of major ecological resources over the monitoring region in 2015

Regions	Forest			Grassland		Farmland	
	The forest aboveground biomass (billion tons)	ALAI	MFVC	ALAI	MFVC	ALAI	MFVC
Russia	923	1.26	0.98	0.63	0.91	0.95	0.92
Europe	298	1.65	0.94	0.98	0.87	1.36	0.89
Southeast Asia	218	3.64	0.99	2.67	0.97	2.05	0.93
South Asia	72	2.18	0.92	0.34	0.51	0.89	0.76
Central Asia	9	0.89	0.86	0.37	0.67	0.48	0.78
West Asia	25	1.33	0.77	0.49	0.51	0.46	0.51
East Asia	248	1.81	0.99	0.50	0.83	1.03	0.93
Northern Africa	109	0.90	0.65	0.31	0.37	0.60	0.56
Southern Africa	751	2.13	0.87	1.19	0.74	1.12	0.76
Oceania	160	1.16	0.63	0.70	0.58	0.98	0.80

Table 1–3 Anomaly of major ecological resources in 2015 compared with the mean from 2010 to 2015

Area	Forest			Grassland anomaly(%)		Farmland anomaly(%)	
	The forest aboveground biomass (billion tons)	ALAI (%)	MFVC (%)	ALAI	MFVC	ALAI	MFVC
Russia	21	–0.44	0.67	–0.52	1.51	2.17	2.09
Europe	2	3.94	0.45	2.27	–0.24	5.13	0.96
Southeast Asia	–5	3.48	0.56	1.78	0.84	4.06	1.22
South Asia	2	5.48	0.72	7.59	1.43	4.10	0.53
Central Asia	0	4.31	3.00	7.51	7.51	8.25	7.05
West Asia	1	4.89	2.39	5.00	6.31	8.83	7.63
East Asia	17	4.65	0.69	0.76	–2.19	5.60	0.49
Northern Africa	–2	4.41	1.02	6.03	0.78	4.08	0.98
Southern Africa	–11	2.37	–0.32	1.16	–0.86	0.62	–0.30
Oceania	1	1.01	1.46	–3.79	–1.55	–1.97	1.78

2. Ecological environment and development conditions of critical urban areas

The monitoring area includes the area along 17 important cities of six primary economic corridors of the 'Belt and Road' , 5 urban areas in Africa and 1 in Oceania (Fig. 2–1). The monitoring was conducted by administrative unites or 150 km around the core city as boundary.

Based on the indices of land cover, nightlight index and heat island intensity, the regional development and ecological environment of these critical cities are evaluated (Table 2–1).

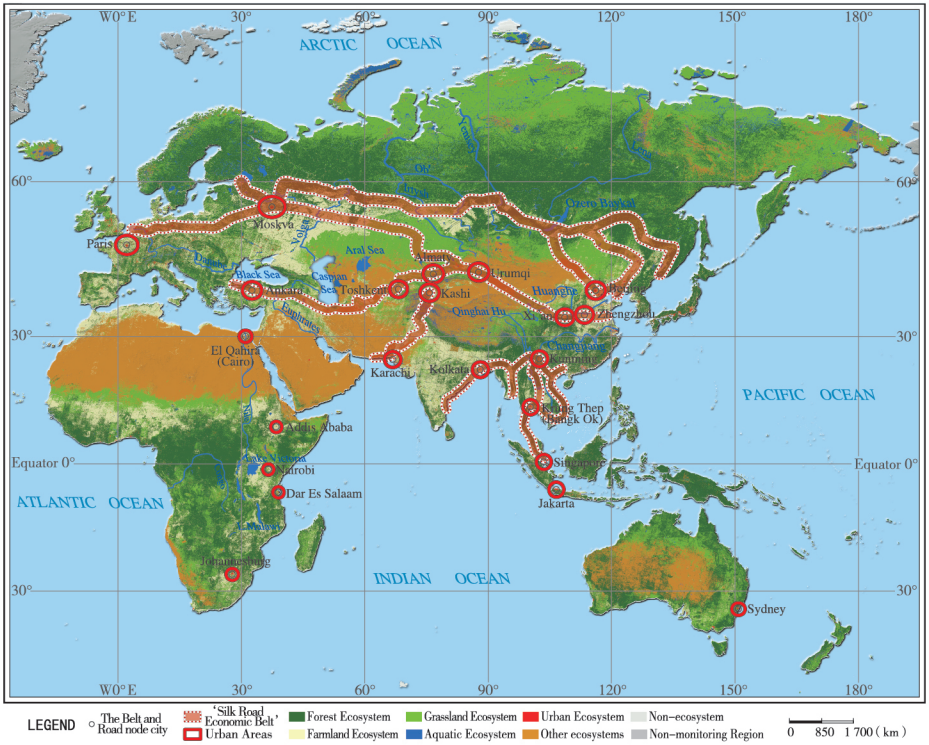

Fig. 2–1 Spatial distribution of major urban areas in the 'Belt and Road' region

The nine urban areas, Beijing–Tianjin–Hebei, Moscow, Central China, Paris, Singapore, Jakarta, Bangkok, Cairo, Johannesburg, either being the national capital or critical metropolis along the 'Belt and Road' , are the advanced and developed cities, which have high proportion of urban built land, high city scale and land development intensive, more than 9 of urban area nightlight index, higher social and economic development level, and play an important leading role in the strategic implementation of the 'Belt and Road' . During 2000–2013, the annual rate of nightlight index increased by above 0.3 in the Beijing–Tianjin–Hebei region, Moscow, Central China, Bangkok and Cairo, indicating a higher pace of development and a greater potential for future development (Fig. 2–2). While the annual increase rate of nightlight index in Paris, Singapore, Jakarta and Johannesburg has also increased but lower than 0.3, implying slower development progress in recent years (Fig. 2–3). The development vitality is much less compared to that of the former categories, and further revitalizing the potential of urban development and creating new economic growth points is the key to the vitality of such urban areas.

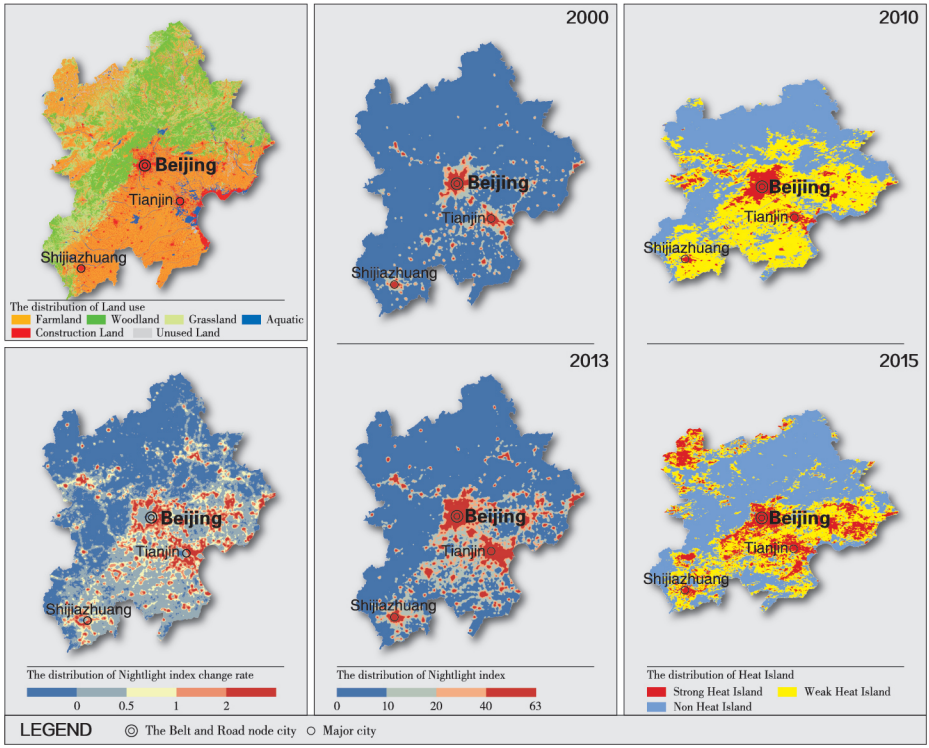

Fig. 2–2 Environmental indicators of Beijing–Tianjin–Hebei, China

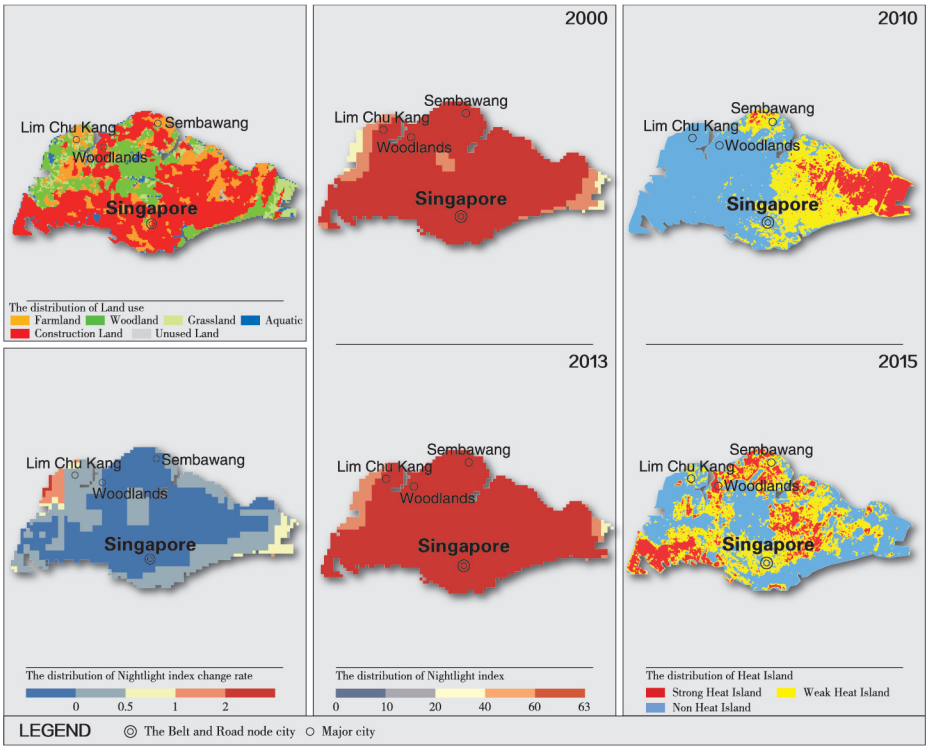

Fig. 2–3 Environmental indicators of Singapore

The seven urban clusters, namely the central Shaanxi plain, Northern Slopes of Tianshan Mountains, Istanbul, Ankara, the central region of Yunnan Province, Kolkata and Kashgar, represent the rapidly growing areas of developing countries along the 'Belt and Road', demonstrated a moderate level of development among the 23 urban clusters, and the annual growth rate of the nightlight index stayed above 0.15 since 2000. These urban clusters have a great development potential (Fig. 2–4, Fig.2–5, Fig 2–6). Through strengthening infrastructure and cooperation and exchanges, these urban areas are expected to become the new growth poles and spot lines of the 'Belt and Road'.

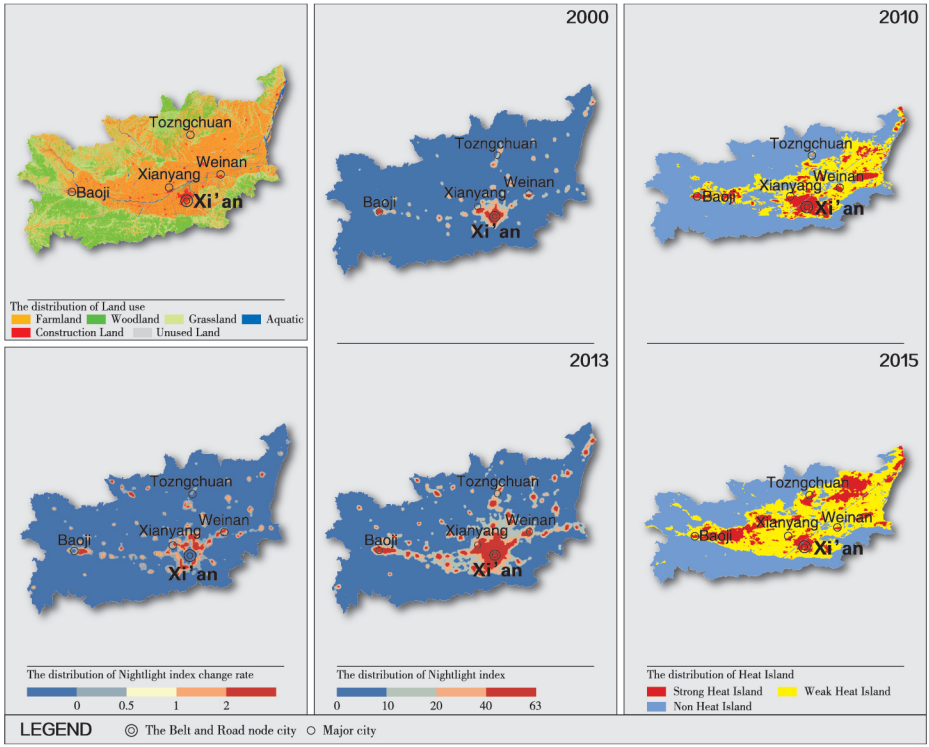

Fig. 2–4 Environmental indicators of the central Shaanxi plain, China

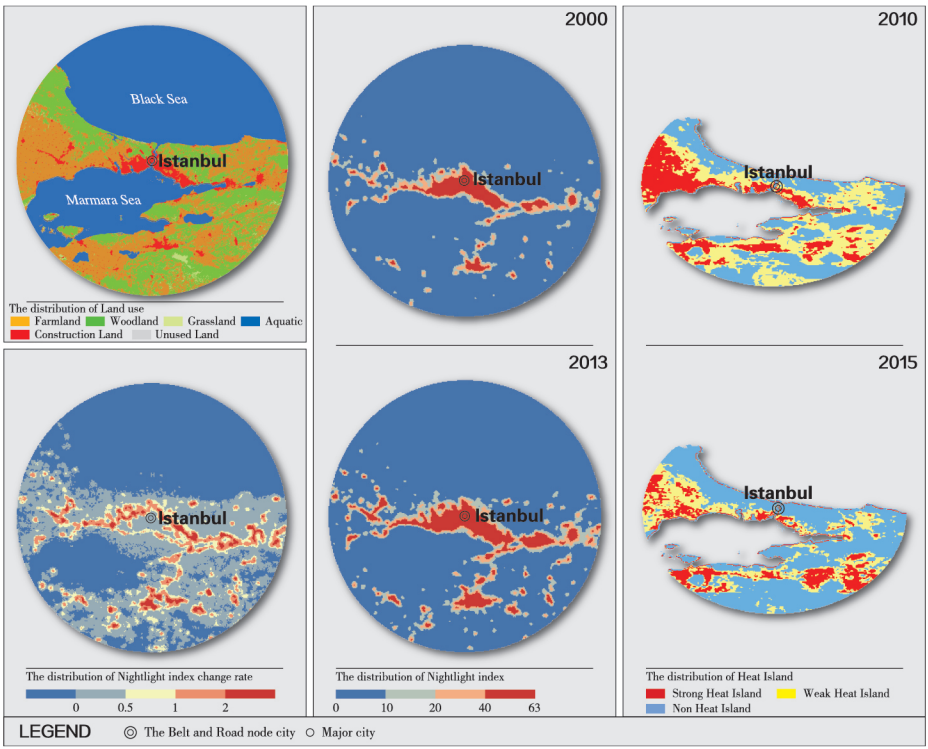

Fig. 2–5 Environmental indicators of Istanbul, Turkey

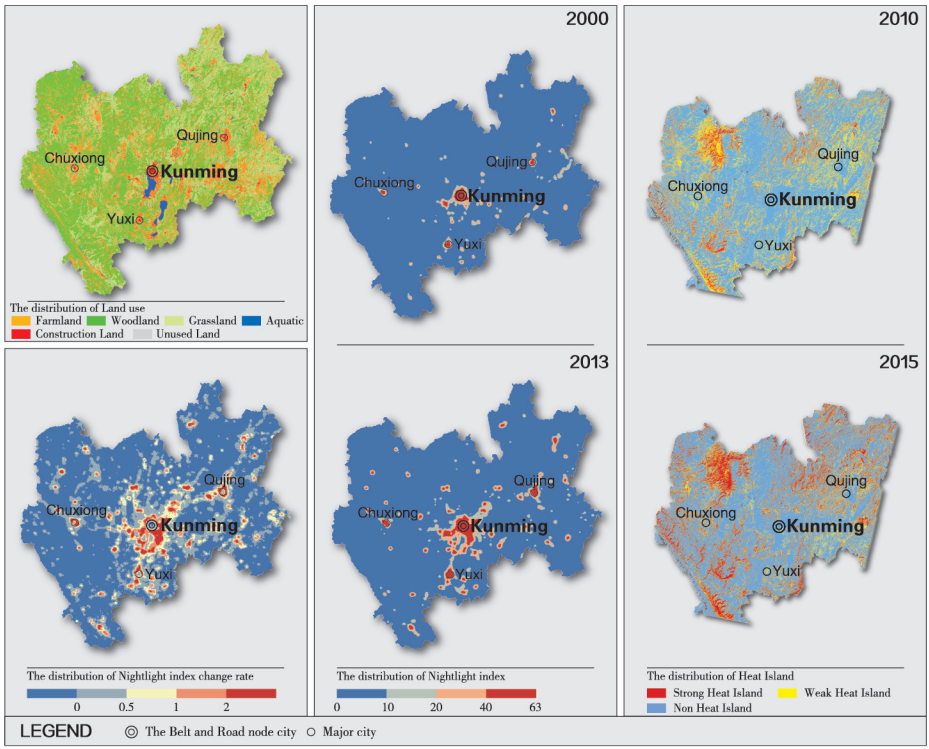

Fig. 2–6 Ecological environment and development condition of the central region of Yunnan Province, China

Even less developed are the following seven urban areas, namely Alma–Ata, Tashkent, Karachi, Nairobi, Dar–Es–Salam, Addis Ababa. These are major port cities or smaller cities along the 'Belt and Road' , and the annual growth rate in nightlight index is lower than 0.1 (Fig. 2–7, Fig. 2–8). These small cities appear to be lack of development vitality along the 'Belt and Road' and require future strengthening in infrastructure to narrow the gap with developed cities should be a specific task for the construction of the 'Belt and Road' .

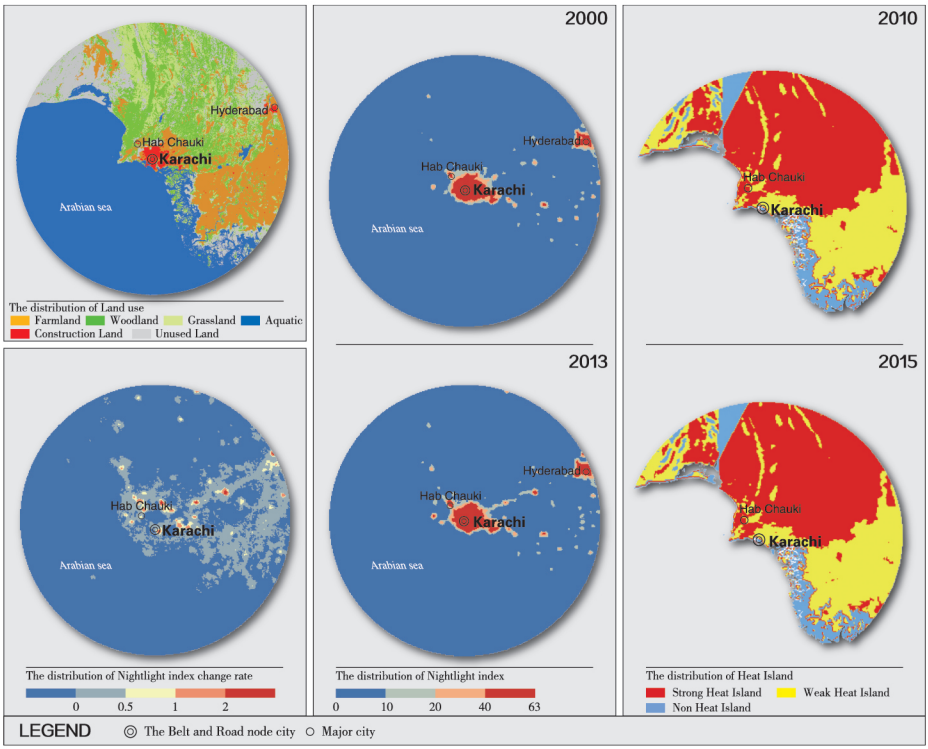

Fig. 2–7 Environmental indicators of Karachi, Pakistan

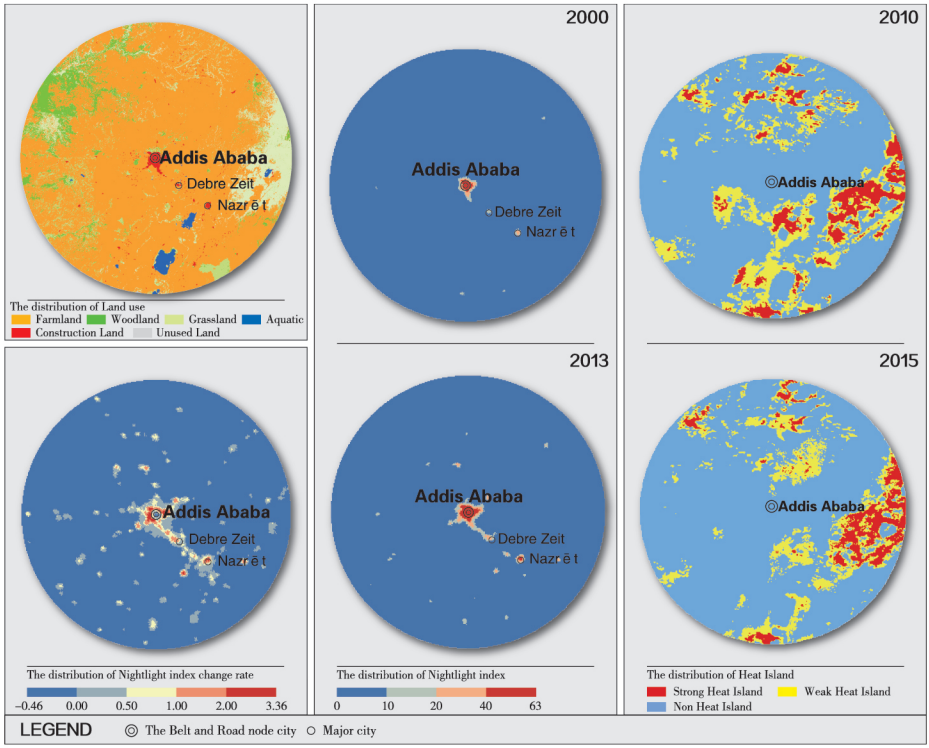

Fig. 2–8 Environmental indicators of Addis Ababa, Ethiopia

Table 2–1 Land use type area ratio / nightlight index / nightlight index change rate and hot island area ratio of major urban areas

Economic corridor or region	Urban areas	Area ratio (%)				Nightlight index in 2013	Nightlight index change rate 2000–2013	Area ratio (%)		
		Farm land	Wood land	Grass land	Construction land			Strong heat island	Weak heat island	Not heat island
China–Mongolia–Russia	Beijing–Tianjin–Hebei	45.16	23.92	17.51	9.18	10.25	0.39	14.35	30.43	55.22
	Moscow	43.07	44.28	1.22	10.43	16.62	0.46	9.66	22.42	67.91
New Eurasian Continental Bridge	Central China	65.82	13.92	6.46	11.64	9.12	0.38	3.42	17.48	79.1
	The central Shaanxi plain	44.25	23.79	24.56	5.69	7.85	0.35	12.16	34.03	53.81
	Paris	74.55	16.05	1.07	8.08	14.74	0.25	8.85	35.73	55.42
China–Central Asia–West Asia	Northern slope of Tianshan Mountain	16.75	4.53	42.56	2.27	3.21	0.15	25.29	24.55	50.16
	Alma–Ata	26.88	5.73	52.8	1.79	1.75	0.08	39.08	21.09	39.83
	Tashkent	44.81	7.61	36.71	5.25	3.65	0.03	26.1	36.84	37.07
	Istanbul	24.52	20.35	1.02	3.94	7.15	0.23	20.82	38.55	40.63
	Ankara	56.35	20.97	18.53	1.91	3.84	0.14	23.04	38.72	38.24
China–Indo–china Peninsula	Singapore	16.59	19.97	6.54	52.52	62.42	0.09	21.15	28.63	50.22
	Bangkok	66.06	10.46	1.35	2.66	15.81	0.48	18.36	31.51	50.13
	Jakarta	33.1	24.25	1.59	4.88	12.47	0.27	13.42	28.42	58.16
Bangladesh–China–India –Burma	the central region of Yunnan Province	20.86	49.43	26.74	1.63	3.49	0.16	18.77	24.65	56.58
	Calcutta	63.89	6.61	1.12	14.73	7.52	0.19	4.13	32.7	63.17
China–Pakistan	Kashga	39.6	0.33	13.02	2.32	3.45	0.2	4.36	34.21	61.43
	Karachi	14.55	16.78	9.87	1.05	2.22	0.02	8.82	38.41	52.76
Africa and Oceania	Dar–Es–Salaam	7.86	19.99	12.69	0.76	0.65	0.02	11.2	47.91	40.88
	Cairo	40.98	0.35	0.11	2.39	20.31	0.61	23.66	41.43	34.91
	Nairobi	57.55	17.96	22.46	0.29	1.4	0.05	17.47	32.02	50.51
	Addis Ababa	79.4	13.8	4.96	0.43	0.69	0.03	5.38	13.04	81.58
	Johannesburg	36.7	33.26	20.69	8.27	10.65	0.19	1.32	35.84	62.84
	Sydney	6.86	37.67	9.6	3.05	4.14	0.04	1.63	12.05	86.32

3. Road connectivity conditions

3.1 Road network density distribution and road capacity

The highway network density of monitoring area is averaged at 244 m/km^2, but with a high spatial variability across the region, higher in the coastal regions and lower in inland areas. There is a high correlation between highway network density and regional population density also the degree of socioeconomic development (Fig. 3–1). Areas of highway density are concentrated in Europe, southeast coast of China, Japan, southern Australia, coastal areas of India and Africa. Europe has the highest road network density, followed by the southeast coast of China and Japan. Much of the monitoring region is seen to have low to moderate road network density and the coverage rate is gradually decreasing from the coastal region to the inland.

The railway network density of the monitoring area is averaged at 12 m/km^2, much less than the density of highway network. The spatial pattern resembles that of highway network density (Fig. 3–2) : railway network density is significantly higher in the coastal area than in inland areas, higher within developed countries than in developing countries. Again, Europe has the highest railway density than any other regions in the monitoring area, Africa is clearly lagging behind, with some nations absent of any railway networks.

The 'Belt and Road' Initiative begin geographically in East Asian economic circle and ends in European economic circle. In between, the road networks in India are also seen to be highly developed. However, there is clearly a lack of connectivity between China and India, and between India and Europe. The road capacity index of the entire area is 138m/km^2, while the indices of Europe, eastern China and India are 615 m/km^2, 541 m/km^2, 340 m/km^2 respectively, 60% above the average (Fig. 3–3).

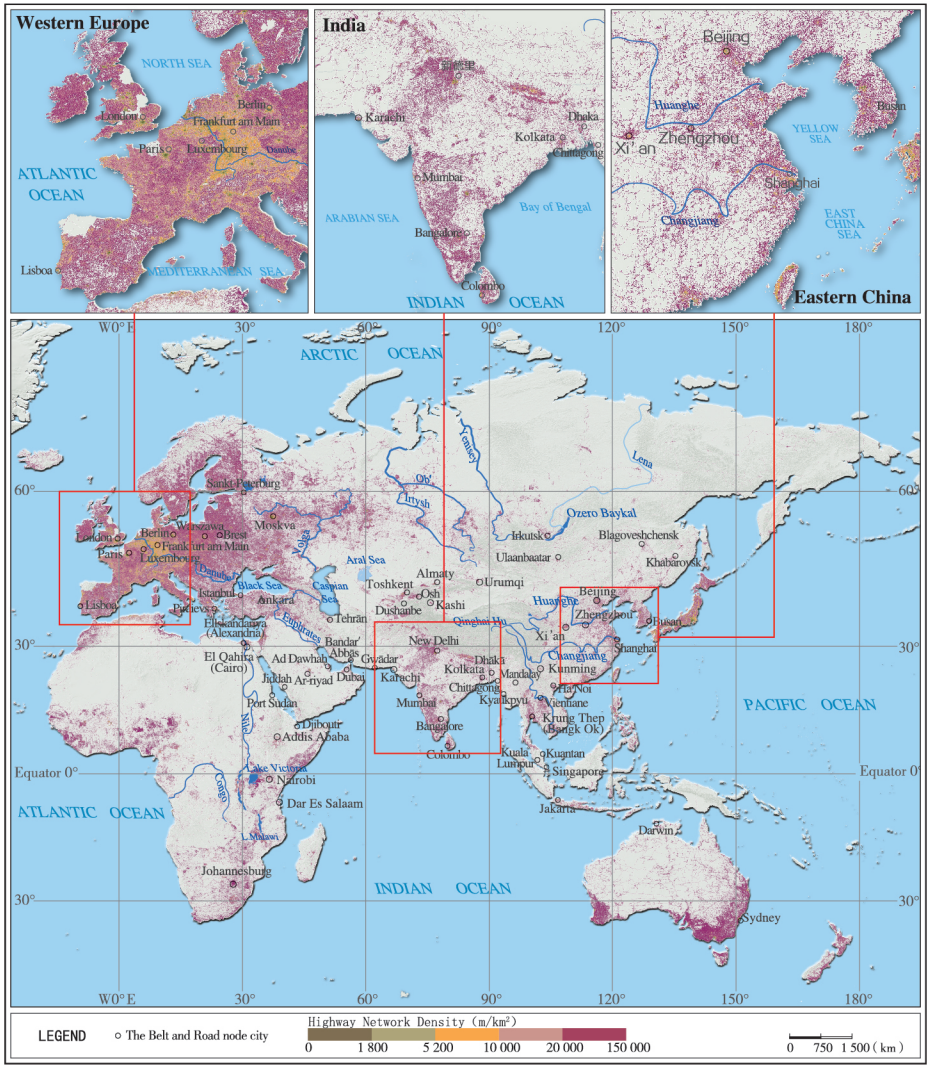

Fig. 3–1 Distribution of highway network density in monitoring area

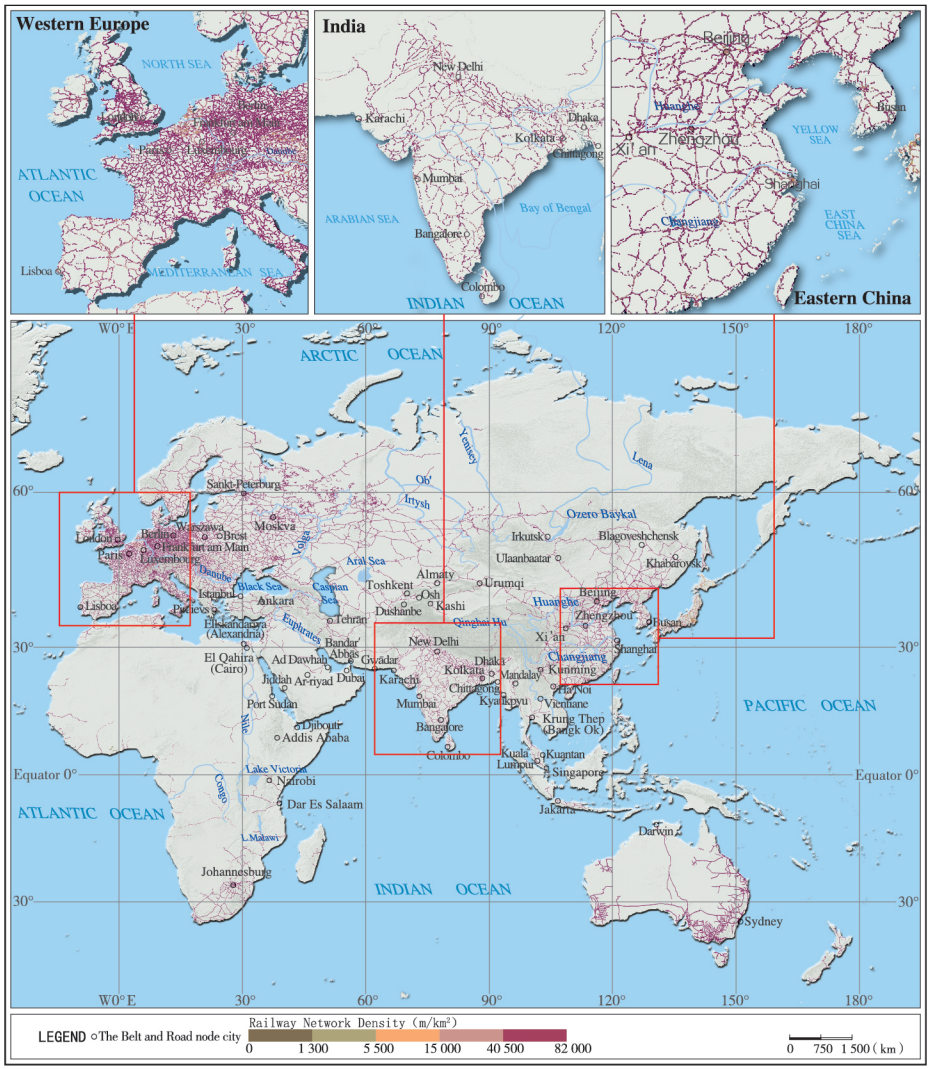

Fig. 3–2 Distribution of railway network density in monitoring area

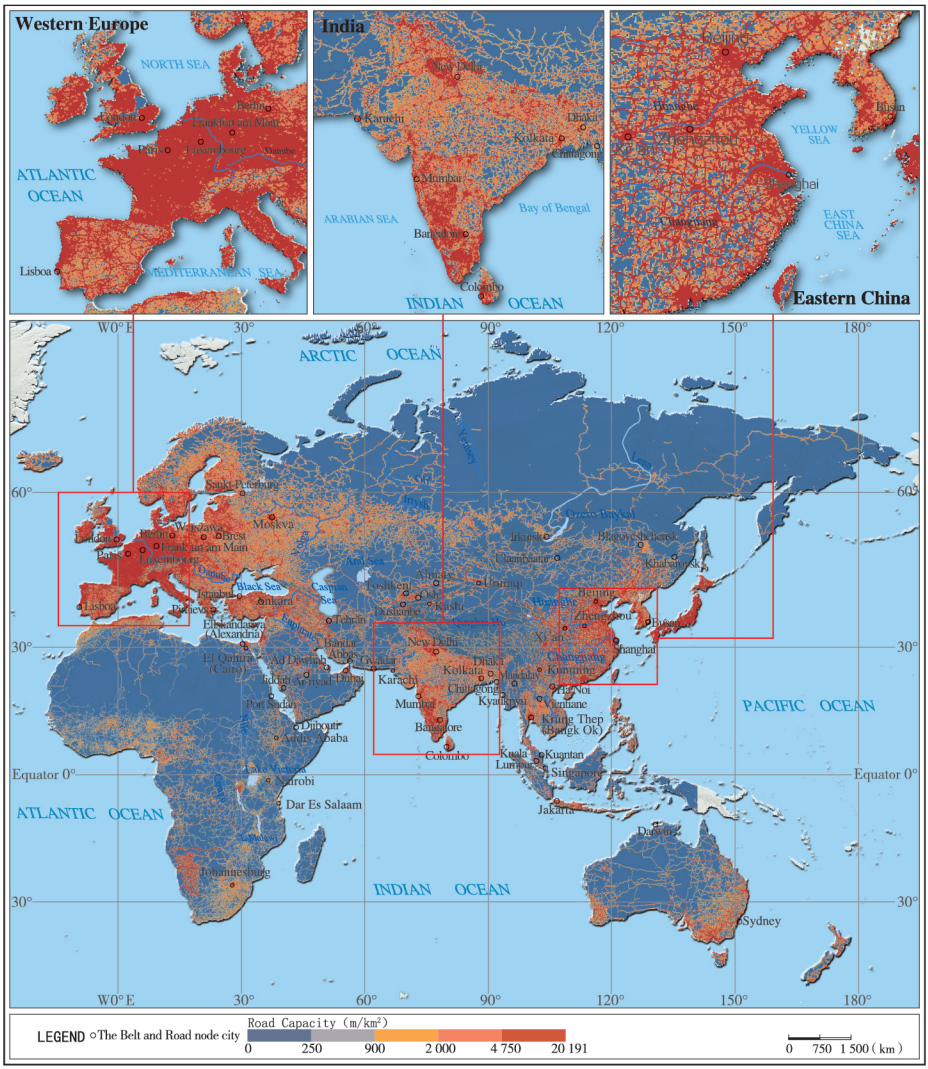

Fig. 3–3 Distribution of the road capacity index in monitoring area

3.2 Road accessibility of economic corridors

The areas of good road capacity and accessibility are concentrated at both ends of the China–Mongolia–Russia economic corridor and the new Eurasian Continental Bridge. Due to cold climates, rugged terrain, desert environment, and other unfavorable geographical factors, poor road capacity and accessibility is seen in the central region of China–Mongolia–Russia economic corridor and the central region of the new Eurasian Continental Bridge. These unfavorable factors are largely responsible for the lower road capacity and accessibility in China–Central Asia–West Asia economic corridor and China–Pakistan economic corridor. The road capacity and accessibility are generally more balanced in China–Indo–China Peninsula economic corridor and Bangladesh–China–India–Burma Economic Corridor (Fig. 3–4).

Fig. 3–4 Road accessibility of economic corridor

3.3 Impact of road constructions on landscape

Road constructions inevitably cause fragmentation of landscape therefore impose a negative impact on ecosystem integrity. This negative impact can be as high as 10% in landscape fragmentation for roads constructed within/cross the ecologically fragile areas(ecotones) of the China–Central Asia–West Asia economic corridor and the new Asia–Europe continental bridge economic corridor (shrub desert and other ecotones such as temperate mixed forests, temperate needle–leaved forest–grassland, montane grassland, etc.). Within these six economic corridors, landscape fragmentation is similar under the two scenarios: with or without road constructions (Table 3–1). The impact of the road varies around 10% and the greater the current fragmentation of landscape, the smaller the impact of road constructions. In irrigated areas of China, deserts/shrub areas of eastern Central Asia and Pakistan, and mangrove forests of Myanmar along the economic corridor of the 'Belt and Road', the impact of road on landscape fragmentation is seemingly apparent.

Table 3–1 Economic corridor fragmentation and road impact ratio

Economic corridor	Fragmentation no road	Fragmentation of roads	Road affects proportion (%)
China–Mongolia–Russia economic corridor	0.3839	0.4065	7.32
New Eurasia Continental Bridge	0.8327	0.9644	12.55
China–Central Asia–West Asia economic corridor	0.6791	0.7774	14.62
China–Indo–china Peninsula economic corridor	0.5718	0.6362	8.98
China–Pakistan economic corridor	1.5409	1.5850	3.28
Bangladesh–China–India–Burma economic corridor	1.3549	1.5127	9.35

4. Status of terrestrial solar energy resources

4.1 The spatio–temporal distribution of solar radiation

The spatial distribution of solar energy resources is influenced mainly by latitude, topography and cloud cover, while the latter is usually more profound. Regions in lower latitude are endowed with the most abundant solar radiation. Africa, South Asia, West Asia, Oceania, with annual average solar radiation of greater than 6,500 MJ/m^2/a, and the seasonal variability is insignificant. In Southeast Asia, Central Asia, East Asia, solar energy resources are also abundant, with annual average solar radiation of greater than 5,300 MJ/m^2/a, followed by Europe (4,300 MJ/m^2/a). Russia is less endowed with solar radiation resources due to its higher latitude and it is only averaged at 3,093 MJ/m^2/a while the annual variation is high (the solar radiation in July is ten times that in December). The Tibetan Plateau enjoys less solar radiation compared to Central Asia although with the same latitude, primarily because of higher cloud cover (6,300 MJ/ m^2/a) (Fig. 4–1).

4.2 Photovoltaic power potential and development status

Photovoltaic (PV) power potential is mainly determined by annual global solar radiation, seasonal variation, land surface types and transportation factors, among others. Areas suitable for solar power development are mainly located within low latitude desert and sparsely vegetated areas, including West Asia, the Sahara desert and Kgalagardi desert of Northern Africa, Kgalagardi desert in Southern Africa and central and western regions of Australia, where the annual PV power potential is greater than 350 KWh/m^2. In Southeast Asia and in South Asia(India), large–scale development of solar energy is not suitable due to its high vegetation coverage of farmland and forests. Russia has the least solar potential due to its high latitude and natural geographical conditions (Fig. 4–2).

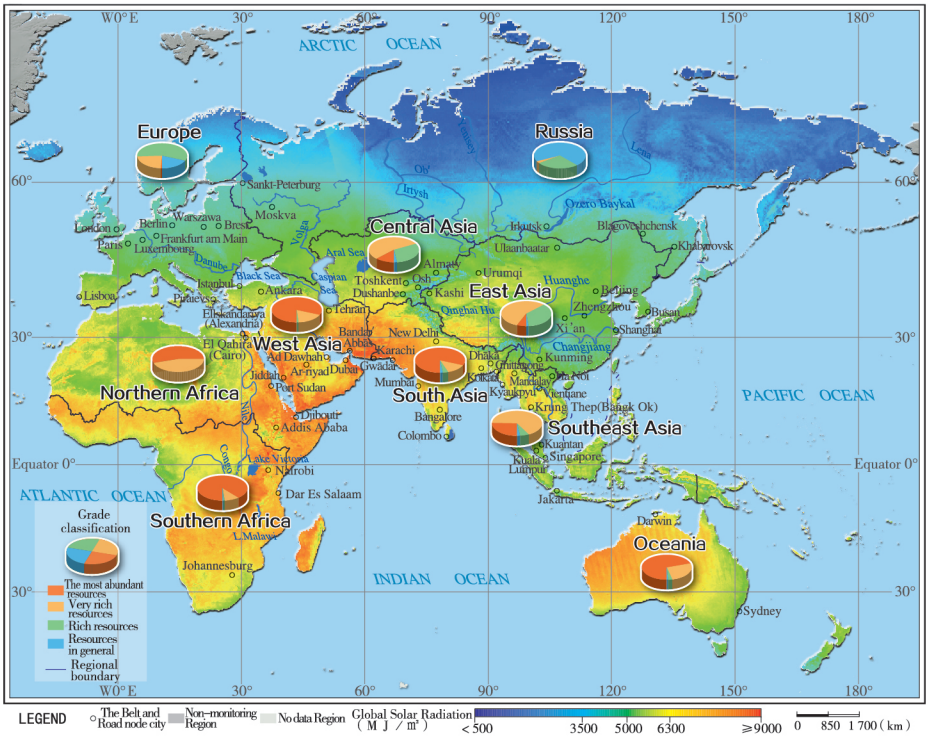

Fig.4–1 Distribution of solar energy resources level of the 'Belt and Road' region in 2015

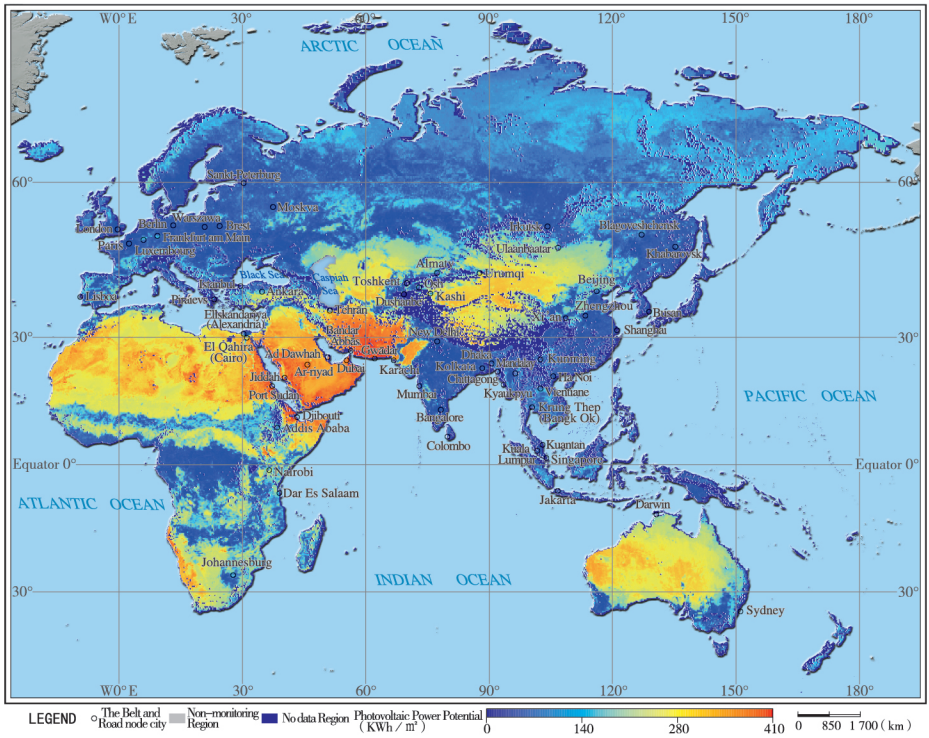

Fig.4–2 PV power potential of the 'Belt and Road' region in 2015

International action to combat climate change, energy policy, natural conditions and economic development level are the major determinants of the solar industry development. Due to the active response to climate change and new energy policy, China is leading the world in PV developments. Australia is abundant in solar resources and it has already become the eighth largest PV market owning to national policy support, and there is still a huge potential for future development. Currently five European countries are among the world's top 10 PV installations, as a result of the implementation of "roof project", and are expected to maintain higher levels of future distributed PV power generation. PV power generation in Africa is much less developed although its solar resources endowment is high. The oil–rich countries in West Asia, do not currently favor PV generation, simply because energy is not a limiting factor in socioeconomic development (Table 4–1).

Table 4–1 PV capacity, solar power potential and economic status statistics

Nations	Affiliating area	PV capacity (Photovoltaic permeability of total power demand)	PV power potential (10^3 × TWh)	GDP (10^3 × billions dollars)	Per capita generation potential (10^4 × KWh)	Per capitaGDP (10^3 × billions dollars)	Per capita electricity consumption (10^2 × KWh)
China	East Asia	78.1(1.8%)	1055.8	110.1	77.0	8.0	39.1
apan		42.8(4.9%)	4.9	43.8	3.8	34.5	78.4
South Korea		4.4(1.15%)	1.5	13.8	2.9	27.2	105.2
GermanyS	Europe	41.2(7%)	11.5	33.6	14.1	41.3	88.8
Italy		19.3(7.3%)	7.0	18.2	11.6	30.0	50.0
England		11.6(3.4%)	5.0	28.6	7.7	43.9	50.9
France		7.1(1.63%)	22.9	24.2	34.3	36.2	68.9
Spain		5.5(3.33%)	27.6	12.0	59.5	25.8	53.6
Belgium		3.4(4.25%)	0.8	4.6	6.7	40.3	76.6
Greece		2.6(7.4%)	3.5	1.9	32.5	18.0	50.9
The Netherlands		2.1(1.78%)	0.7	7.5	4.2	44.3	66.8
Czech		2.1(3.4%)	1.6	1.9	15.6	17.5	62.4
Switzerland		1.6(2.83%)	1.7	6.7	20.3	80.9	74.3
Romania		1.5(2.88%)	8.5	1.8	43.0	9.0	25.9
Austria		1.1(1.78%)	2.8	3.8	32.4	43.8	82.9
Denmark		0.9(2.75%)	0.3	3.0	5.2	52.0	58.3
India	South Asia	9(1.55%)	126.8	21.0	9.7	1.6	8.0
Pakistan		1.7	153.8	2.7	81.4	1.4	4.6
Thailand	Southeast Asia	2.2(1.93%)	27.0	4.0	39.7	5.8	25.6
Philippines		0.9	6.3	2.9	6.2	2.9	7.0
Israel	West Asia	0.9(2.85%)	3.8	3.0	45.5	35.7	64.7
Turkey		0.8(0.48%)	75.8	7.2	96.4	9.1	39.0
Australia	Oceania	5.9(3.85%)	1563.9	13.4	6576.4	56.3	99.4
South Africa	Africa	1.5(1.03%)	197.1	3.1	358.6	5.7	41.7

* The PV capacity data and PV permeability data of total power come from 2016 global PV market express of PVPS (PV power system project); electricity consumption data from IEA(International Energy Agency)

5. Terrestrial water budget

5.1 The spatio–temporal distribution of water budget

In Central Africa, southeast region of East Asia and Southeast Asia, the precipitation is abundant, with the annual amount of over 1,200 mm, 1,600 mm and 2,000 mm in 2015 respectively, and the water surplus is above 200 mm, 600 mm and 1,000 mm respectively. In Central Asia, West Asia and North Africa with arid climate, the precipitation is below 200 mm, and the precipitation and evapotranspiration are in balance (Fig. 5–1).

Fig.5–1 The distribution of water deficit over the 'Belt and Road' in 2015

In the desert oases and the irrigated agricultural area with intensive water use, the precipitation cannot meet the demand of water consumption for the farmland evapotranspiration, and the competition between water for agricultural and ecological requirement is prominent, resulting in a severe water crisis. In oasis areas along the silk road with water deficit of 500 mm/a, such as the Hexi Corridor and Trim

River basin in China and the Syr Darya River basin in central Asia, the sources of water for the evapotranspiration are mainly from snow/glacier melt in the alpine region surrounding the basins. The ecological water requirement cannot be met because more water is used for oasis agricultural production, leading to ecological degradation and land desertification. In northwestern India and north China plain, evapotranspiration is significantly higher than precipitation over irrigated agricultural areas, with the water deficit of 200 mm. Diverting surface water from the Ganges, Yellow River and other water bodies, or by overexploiting groundwater has caused a significant decrease in underground water level, land subsidence, and ecological degradation. (Fig. 5–1, Fig. 5–2)

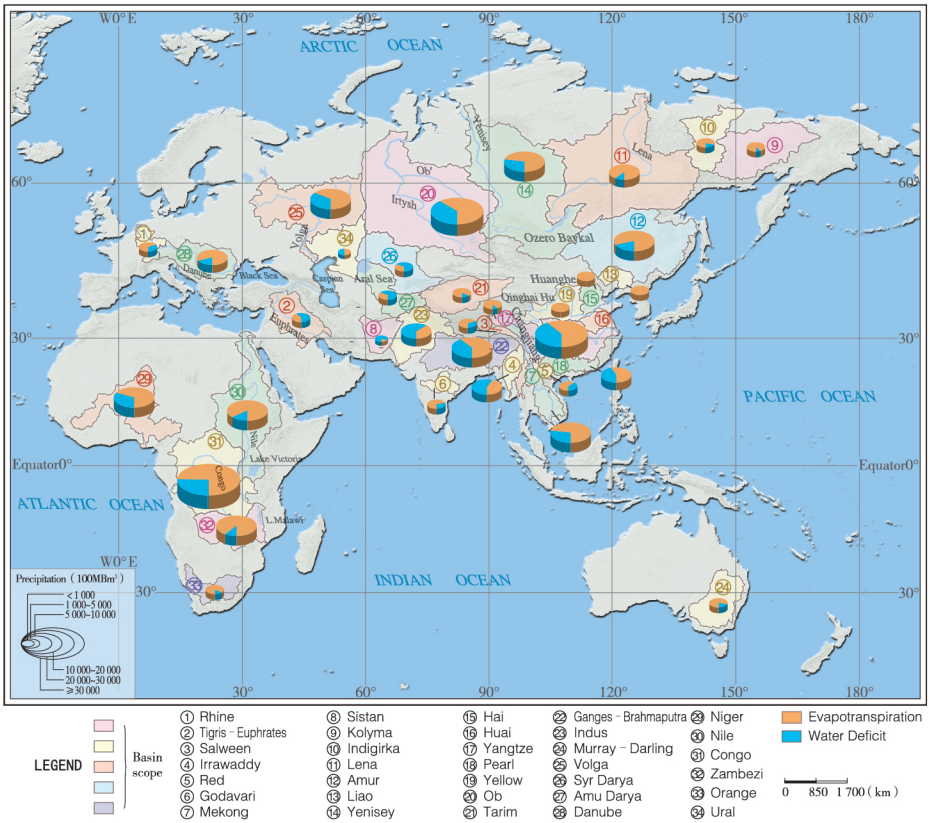

Fig.5–2 Water budget of the different basins along the 'Belt and Road' in 2015

5.2 The effects of *El Niño* on regional water budget in 2015

The super *El Niño* from October 2014 to April 2016 resulted in a huge reduction in precipitation leading to severe droughts in 2015. Affected by warming anomaly of sea surface temperature over the east Pacific and Indian Ocean, the atmospheric convective activity on both west banks of these oceans were significantly weaker, the annual precipitation is reduced on average by 20.5%, 14.7% and 12.1% in Oceania, Southeast Asia and Southern Africa. At the basin level a reduction of 35.9% is observed in the Orange River basin, 21.3% in the Malay Archipelago in southeast Asia, 20.1% in the Murray–Darling River basin in Australia, resulting crop reduction, shrinking of wetland, and widespread of wildfires. In addition, the water level of reservoir has decreased sharply, leading to a significant reduction in power generation as a result (Fig.5–3, Fig.5–4).

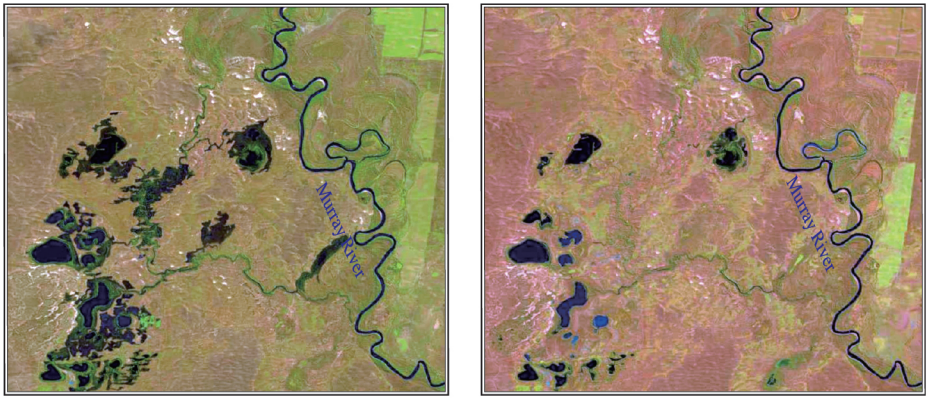

（a）July 30, 2014　　（b）June 02, 2015

Fig.5–3 Landsat 8 OLI image of the Hattah–Kulkyne national park wetland change (shrinking and degradation) in Australia for 2015

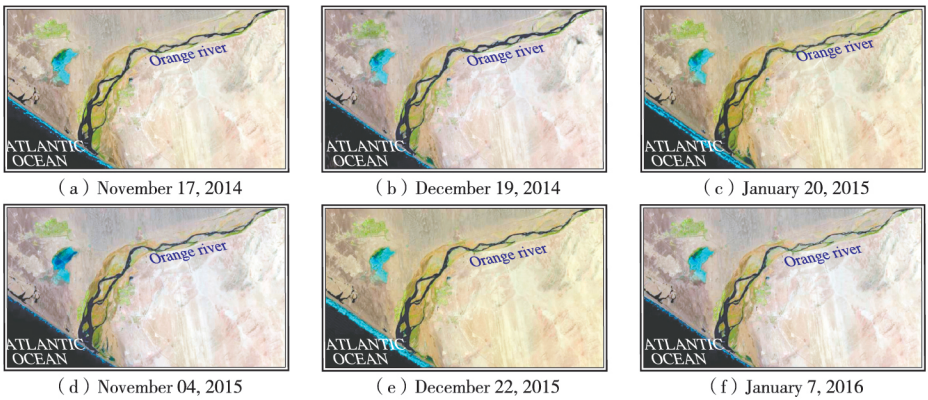

(a) November 17, 2014 (b) December 19, 2014 (c) January 20, 2015

(d) November 04, 2015 (e) December 22, 2015 (f) January 7, 2016

Fig.5–4 Landsat 8 OLI image of river water surface changes (narrowing down) near the estuary of the Orange River in Southern Africa for 2015

6. Typical Marine disasters in key ocean areas

6.1 The spatio–temporal distribution of disastrous waves

In the surrounding area of the three ocean–based 'Blue Economic Passages', the disastrous waves are concentrated near 40° N in the northwestern Pacific Ocean between October and April and the 55° S westerly wind belt in the south–west Pacific and Indian Ocean between February and November (Fig. 6–1). In the recent 10 years, the frequency of disastrous waves in the Black Sea and the Arabian Sea has demonstrated an increasing trend, while at decreasing trend is observed over other areas (Table 6–1).

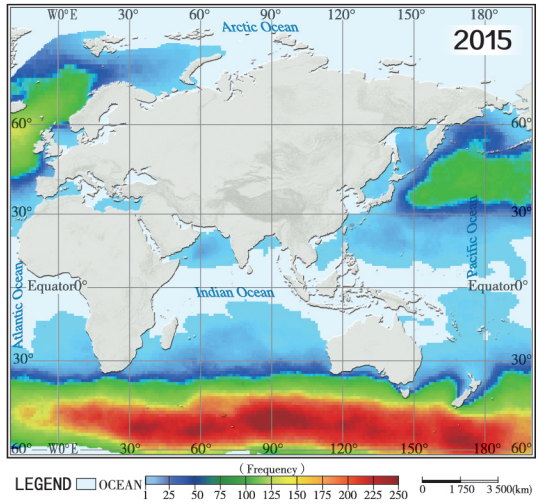

Fig. 6–1 Occurrence frequency distribution of disastrous waves in 2015

Table 6–1 The annual frequency of disastrous waves for 2006–2016

	2006	2007	2008	2009	2010	2011	2012	2013	2014	2015	2016	Average
Japan sea	14	14	15	16	10	7	10	11	7	12	7	11.18
East ChinaSea	9	9	12	11	5	9	9	15	11	5	6	9.18
South China Sea	20	15	16	14	9	18	9	10	10	10	12	13
Java–banda Sea	0	0	0	0	0	0	0	0	0	0	0	0
Bay of Bengal	6	6	5	5	0	4	3	3	4	4	2	3.81
Arabian Sea	39	35	38	29	30	17	14	48	46	29	29	32.18
Mediterranean	6	15	8	16	6	4	4	10	4	7	4	7.63
Black Sea	2	1	2	0	1	4	5	0	0	0	1	1.45
North Sea	38	45	49	29	21	63	45	46	54	72	39	45.54
Northwest Pacific	102	111	87	106	109	111	108	111	136	93	130	109.45
Southwest Pacific	220	189	206	180	228	192	187	191	207	265	209	206.72
Indian Ocean	242	255	245	247	260	215	247	221	275	279	284	251.81
Regional average	58.16	57.91	56.91	54.41	56.58	53.67	53.41	55.5	62.83	64.66	60.25	57.66

6.2 The spatio–temporal distribution of sea level anomalies

Overall, a positive anomaly has been observed in sea level change. The highest positive anomaly is in Java – Banda Sea, southwest Pacific Ocean, the Bay of Bengal and South China Sea, with annual average of 6.47 cm, 6.01 cm, 5.89 cm and 5.88 cm (Fig.6–2). There were negative anomalies in local areas, such as the Black Sea areas in 2007, 2008 and 2012, with respective changes of –2.93 cm, –1.62cm and –0.51cm. The amplitude of seasonal variation in sea level anomaly in the East China Sea, South China Sea, the Bay of Bengal, the Arabian Sea and the Javanese Banda Sea ranges from –5cm to 18cm (Table 6–2).

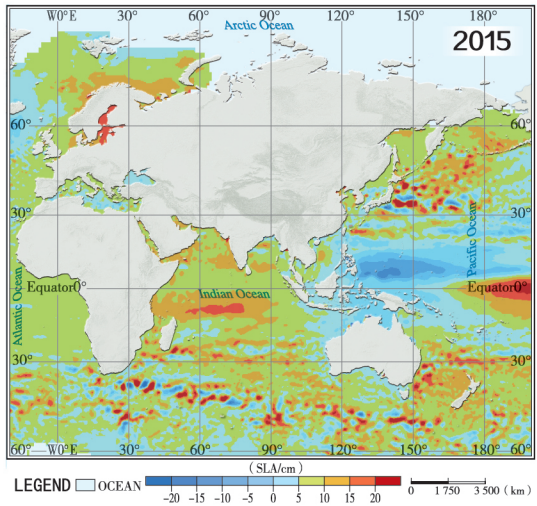

Fig. 6–2 The distribution of sea level anomalies in 2015

Table 6–2 The regional average of sea level anomalies (cm)

	2006	2007	2008	2009	2010	2011	2012	2013	2014	2015	2016	Average
Japan Sea	1.82	4.26	3.33	4.34	5.47	3.77	6.49	5.22	6.40	5.78	10.52	5.22
East China Sea	3.94	2.97	2.98	3.83	4.27	3.38	7.33	5.66	7.55	7.33	9.85	5.37
South China Sea	3.16	2.33	6.12	5.77	7.01	6.26	8.12	8.70	6.07	4.72	6.40	5.88
Java–Banda Sea	1.70	1.98	8.78	6.07	9.25	9.26	9.25	11.03	5.36	0.76	7.72	6.47
Bay of Bengal	0.78	1.05	5.31	4.10	6.97	6.32	7.01	7.66	5.72	7.69	12.18	5.89
Arabian Sea	2.32	3.80	3.88	5.07	4.85	5.59	6.64	6.03	6.01	9.53	9.22	5.72
Mediterranean	2.96	1.81	2.90	4.13	7.47	3.84	4.88	6.65	6.81	5.34	7.18	4.91
Black Sea	3.57	–2.93	–1.62	1.74	12.54	5.43	–0.51	11.57	4.98	3.25	7.15	4.11
North Sea	4.00	6.24	3.57	1.85	1.58	6.59	3.78	4.14	4.33	8.85	7.48	4.76
Northwest Pacific	3.98	4.57	5.77	4.64	4.99	5.99	7.11	6.77	4.58	2.66	5.97	5.18
Southwest Pacific	3.72	4.12	5.31	5.41	5.10	6.29	6.85	6.94	7.73	7.38	7.21	6.01
Indian Ocean	3.76	4.01	5.03	4.77	5.90	5.70	6.44	6.10	6.14	7.32	7.32	5.68
Regional average	2.98	2.85	4.28	4.31	6.28	5.7	6.12	7.21	5.97	5.88	8.18	5.43

6.3 The spatio–temporal distribution of typhoon

Typhoon disasters mainly occur in mid–latitude area, the densest region of which is located in East China Sea and South China Sea, characterized by high frequency occurrence and wide distribution range. The second is the Bay of Bengal and the Arabian Sea. Typhoons that occurs in the 'Blue Economic Passages' are mostly tropical storms. About 21.25% of which are Category of 4 and 5 typhoons affecting the coastal areas. Typhoons occur mainly from July to October, 53.13% of which are high intensity typhoons, while there is only 22.51% high intensity typhoons during January–March period (Fig. 6–3).

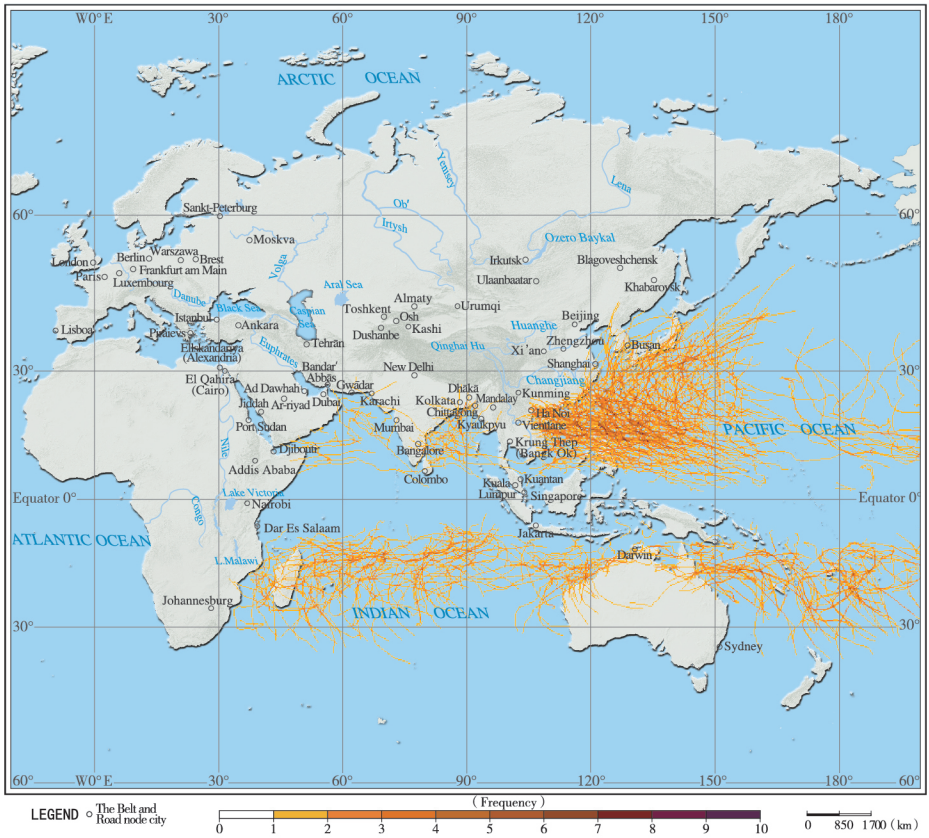

Fig. 6–3 Occurrence frequency distribution of the typhoon disaster (2006~2016)

National Remote Sensing Center of China
Ministry of Science and Technology of the People's Republic of China

Address: Beijing City, South Lane Haidian District Liulin No. 8 Building West Pavilion
Tel：(010)58881180
Fax：(010)58881179
E-mail：webmaster@nrscc.gov.cn
Web：www.nrscc.gov.cn